ELSEVIER

PII: S0032-3861(97)00239-5

Polymer Vol. 39 No. 1, pp. 53–58, 1998

0032-3861/97/$17.00+0.00

Mechanical properties of binary blends of polypropylene with ethylene-α-olefin copolymer

Koh-hei Nitta[a,*], Keikichi Okamoto[a] and Masayuki Yamaguchi[b]
[a]*Center for New Materials, Japan Advanced institute of Science and Technology, 1-1 Asahidai, Tatsunokuchi, Ishikawa 923-12, Japan*
[b]*Yokkaichi Laboratory, TOSOH Corporation, 1-8 Kasumi, Yokkaichi, Mie 510, Japan*
(Received 6 November 1996; revised 28 January 1997)

The compatibility of isotactic polypropylene and ethylene-1-butene copolymers changes with the content of 1-butene in the copolymer so that the morphology of their blends changes drastically. The relationship between morphology and mechanical properties for blends of isotactic polypropylene and ethylene-1-butene copolymer are investigated using a rheo-optical technique; the infrared absorbance spectroscopy and the stress are measured simultaneously under a constant rate of elongation. It is found that the compatible blends affinely deformed accompanied by little plastic deformation such as microvoids and craze, whereas the incompatible blends occurring a phase separation cause a segregation at interface between the two phases in the low strain region.

(Keywords: mechanical properties; isotactic polypropylene; rheo-optical properties)

INTRODUCTION

Tensile properties for blends of polyolefin materials and elastomers are of considerable importance for engineering applications[1,2]. Various elastomers such as ethylene-propylene copolymer, ethylene-propylene-diene terpolymer and butylrubber were used widely for improving the mechanical brittleness of isotactic polypropylene (i-PP) materials[3–6]. The mechanism of the improvement by blending elastomers, however, is not well elucidated on the molecular and structural basis. The main reason for this will be due to lack of systematic studies on the relationship between morphology and mechanical properties.

Our previous study[7] has demonstrated that bulk morphology and microstructure of i-PP can be modified by blending the rubbery ethylene-α-olefin copolymers with wide range of α-olefin contents. Thus, 'α-olefin rich' copolymers are incorporated into the amorphous region of i-PP, whereas 'ethylene rich' copolymers form macroscopically separated domains in i-PP matrix and the domain size largely depends on the α-olefin content and the species of α-olefin. The use of the binary blends of i-PP and ethylene-α-olefin copolymers makes it possible to give a systematic study on the relationship between morphology and mechanical properties.

In this work, the blends of i-PP and ethylene-1-butene copolymer are studied in order to empirically establish a relationship between morphology and mechanical properties. Further, for the better understanding of the effects of morphology on tensile properties, we examined the rheo-optical properties using infrared absorption spectroscopy.

* To whom correspondence should be addressed. Tel. +81-761-41-1451; Fax +81-761-51-1455.

EXPERIMENTAL

Materials

Isotactic polypropylene used in this study was a commercial grade with 3.2 mol% ethylene. The ethylene-α-olefin copolymers were ethylene-1-butene copolymers (EBR) with various 1-butene contents. All the copolymers were essentially random copolymers and rubbery materials. The nomenclature of copolymers is as follows: e.g., EBR36 is ethylene-1-butene copolymer containing 36 mol% 1-butene. The materials used in this study were identical to those used in the previous study[7]. The blend composition of i-PP/EBR was 50/50 (w/w). Details of materials and the blending method were described in the previous article[7]. The i-PP and the blends were melt pressed in a laboratory hot press at 473 K and 10 MPa. The samples quenched at 303 K were prepared for measurements. The thickness of the compression molded samples was adjusted to suitable thickness for measurements.

Polymer characterization

It was found from transmission electron microscopy (t.e.m.) observation[7] that binary blends of i-PP with the 'ethylene rich' copolymers such as EBR36 and EBR45 showed two phases separated and the domain size of EBR36 is larger than that of EBR45, whereas the binary blends of i-PP with the 'α-olefin rich' copolymers such as EBR56 and EBR62 showed a homogeneous phase. Moreover, according to the small angle X-ray scattering and differential scanning calorimetry measurements, the amorphous thickness of the compatible blends, i.e. i-PP/EBR56 and i-PP/EBR62 blends, is larger than that of pure i-PP, whereas the amorphous thickness of the incompatible blends, i.e. i-PP/EBR36 and i-PP/EBR45, is comparable to that of i-PP.

In *Figure 1*, the dynamic mechanical properties of

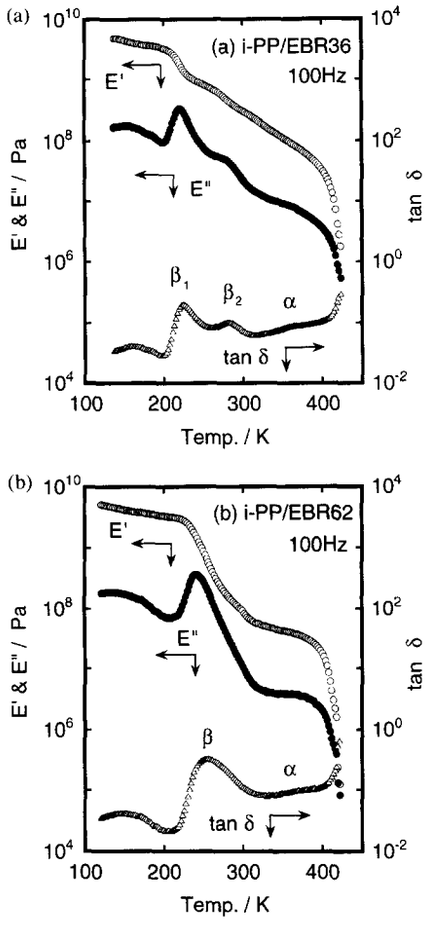

Figure 1 Temperature dependence of dynamic mechanical properties at 100 Hz for (a) i-PP/EBR36 and (b) i-PP/EBR62

i-PP/EBR blends are shown. A heating rate is 2 K min^{-1} and the frequency is 100 Hz. In the incompatible blends, i-PP/EBR36 with phase separated domain, there are two peaks in E″ curves in the temperature range from 200 K to 300 K, which peaks are assigned β_1 and β_2 from the lower temperature. The dispersion at higher temperature β_2 is ascribed to glass-rubber transition of i-PP and the dispersion at lower temperature β_2 is to that of EBR. In contrast, there is only single β dispersion between glass-rubber transition temperatures of the pure component. It is suggested that the EBR molecules are incorporated into the amorphous region of i-PP.

Density for all samples was measured using a flotation method. The binary medium prepared from various ratios of distilled water and ethyl alcohol was used.

The results of characterization of all samples are summarized in *Table 1*.

Table 1 Characteristics of samples

Sample	T_g (K)[a]	T_m (K)[b]	ΔH (J/g)[b]	Density (kg/m^3)
i-PP	280	421	85.9	900
i-PP/EBR36	221(β_1) 281 (β_2)	421	46.7	882
i-PP/EBR45	226(β_1) 274(β_2)	421	44.7	884
i-PP/EBR56	243	420	48.5	892
i-PP/EBR62	243	420	49.3	889

[a]Determined by dynamic viscoelastic measurement. [b]Determined by differential scanning calorimetry.

Tensile measurements

Stress-strain behaviour in uniaxial tension was measured using a Shimadzu AGS-5kN. The sample specimens were cut with a dumbbell shape in which the gauge length is 10 mm. The tensile strain was calculated from the ratio of the increment of the length between clamps to the initial gauge length. The tensile stress was determined from dividing the tensile load by the initial cross section. The stress-strain curves were measured in the range between 243 K and 323 K at a constant strain rate of 0.28% s^{-1} (at a cross-head speed of 5 mm min^{-1}). The strain rate was changed in the range between 0. 11 and 5.56 (% s^{-1}) at 296 K.

Rheo-optical measurements

Rheo-optical techniques afford information on the time dependence not only of the stress-strain but also of optical quantities associated directly with the structure[8,9]. The techniques were developed extensively for crystalline polymers by several investigators[8–13]. In the present study, infrared dichroism and peak frequency shift were measured simultaneously with stress and strain during stretching the film specimen at a constant rate of elongation.

A tensile tester was set in Fourier-transform infrared (*FT*i.r.) spectrometer (JASCO FT-IR500) in such a way as to allow infrared beam go through a film specimen mounted on the tensile tester. The tensile tester was specially designed for upper and lower clamps to symmetrically move from the central point of the film so that the beam spot remains at the initial position during a whole stretching. The strain rate was 0.11% s^{-1} in all cases.

To determine the orientation function of molecular chains and crystal axes, we used the dichroic ratio D which can be determined by $A_\parallel/A_\perp$ where $A_\parallel$ and $A_\perp$ denote the absorbances measured for the radiation whose electric vectors are parallel and perpendicular to the stretching direction, respectively. The Hermans orientation function of molecular chain (or crystal axis) F is related to the dichroic ratio by equation (1)[14–16].

$$F = c\frac{D-1}{D+2} \tag{1}$$

When the direction of the transition moment of the absorption band coincides with the chain axis (or crystal axis), c becomes equal to unity.

The intensities of 998 cm^{-1} and 973 cm^{-1} absorption bands were measured as a function of time or strain every 10 s. The band at 998 cm^{-1} is associated with CH_3 rocking mode as coupled with C–CH_3 stretching mode whereas the band at 973 cm^{-1} is associated with CH_3 rocking mode as coupled with backbone C–C stretching vibrations[17]. The 973 cm^{-1} persists in the melt so that the bands may be closely associated with the amorphous compoment[18,19]. Assuming $c = 1$ for both the 998 cm^{-1} and 973 cm^{-1}, we can estimate the orientation functions of the crystal c-axis and amorphous chain axis of i-PP.

The stressed states of i-PP chains are examined through the measurements of the infrared band shift caused by external stresses. Stress-induced frequency shifts can be interpreted in terms of changes in the potential-energy function due to deformed C–C bonds. The 1168 cm^{-1} was chosen since this band has a large contribution of backbone C–C stretching vibrations of i-PP and is the most sensitive to strains[19,20]. The shifts $\Delta\nu$ appear as a linear function of

the induced stress $\Delta\sigma$ as follows[20,21]:

$$\Delta\nu = \frac{\nu}{b}\gamma_G \Delta\sigma \quad (2)$$

where b is the bulk modulus of chemical repeat units, ν is the frequency of the band, and γ_G the Grüneisen constant[22]. A splain curve fitting operating on the digitally acquired data points gave a reproducibility of peak frequency of around $\pm$ 0.05 cm^{-1} as demonstrated by Wool *et al.*[19,23].

Stress-whitening measurement

It was found that some of film specimens showed stress-whitening during tensile testing. The whitening was easy to observe with eye but was difficult to characterize quantitatively. To obtain a quantitative data of the stress-whitening, we measured the intensity of light transmittance during tensile testing using a He-Ne laser (632.8 nm). The tensile tester described above was mounted on an optical system SALS-100S (IST Planning Co.) in which the laser beam is rendered perpendicular to the stretching direction, passes through the center (stressed regions) of the film and into a photomultiplier. The transmitted intensity was recorded by a transient computer memory as a function of time or strain.

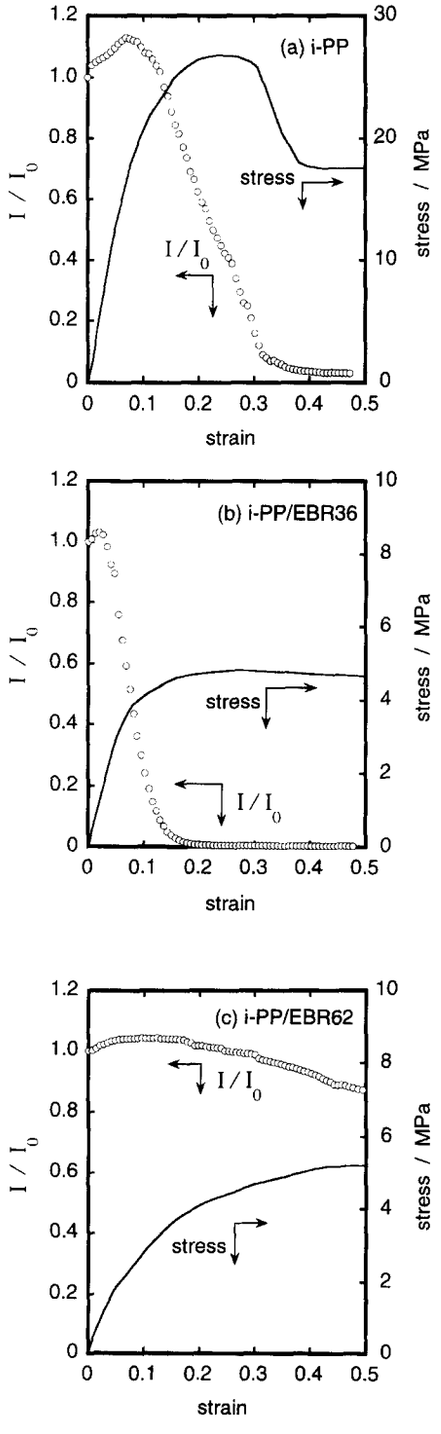

Figure 2 Relative intensity of transmittance of He-Ne laser beam plotted against strain, including stress-strain curves for (a) i-PP, (b) i-PP/EBR36, (c) i-PP/EBR62

RESULTS AND DISCUSSIONS

Stress-whitening

In *Figure 2a–c*, the transmitted intensity I normalized by the initial intensity of unstretched original film I_0 was plotted against strain together with stress-strain curve. The transmitted intensity of i-PP slightly increases in the initial strain region, caused by the film thinning, and drastically decreases with increasing strain. The decrease in the intensity may be caused by the light scattering caused by some entities in the film specimen. The intensity becomes around zero after yielding, suggesting that the stress-whitening of i-PP is directly associated with yielding, i.e., the plastic deformation in deformed spherulite. In the case of the incompatible i-PP/EBR36 blends showing phase separation, as seen in *Figure 2b*, drastic decrease in the intensity occurs in the lower strain regions. The stress-whitening for the incompatible blends may be associated with the segregation at interface between the phases of i-PP and EBR36. Similar results were also seen for i-PP/EBR45 blend. The compatible i-PP/EBR62 having no phase separation showed no stress whitening over the strain ranges as shown in *Figure 2c*. Similar results were obtained for i-PP/EBR56 blend.

Tensile properties

The stress-strain curves of i-PP and i-PP/EBR blends at room temperature are shown in *Figure 3*. The room temperature is above T_g (or β dispersions) of all these samples as shown in *Table 1*. The i-PP sample showed a well-defined yielding and neck formation; it was ductile. The stress-whitening occurred at the strain around 0.3. The incompatible blends such as i-PP/EBR36 and i-PP/EBR45

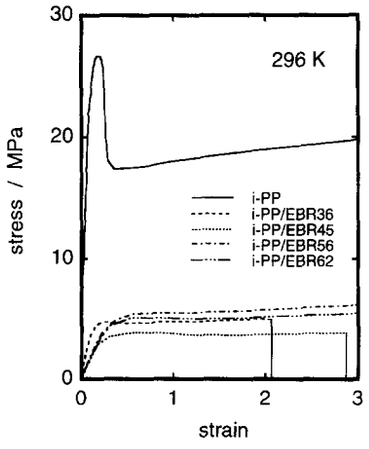

Figure 3 Stress-strain curves at room temperature for i-PP and iPP/EBR blends

immediately showed the stress-whitening and brittle behaviour. The compatible blends such as i-PP/EBR56 and i-PP/EBR62, in contrast, showed no stress-whitening and ductile behaviour. The tensile behaviours at 253 K are shown in *Figure 4*. The temperature is above T_g of EBR56 and EBR62 but is below T_gs of i-PP and/or PP phase in incompatible blends. The transition from ductile to brittle deformation occurred for i-PP. The tensile ductility of compatible blends remains but the stress-whitening occurs in the temperature region below T_g of i-PP. The tensile behaviours of the incompatible blends were similar to those seen at room temperature. *Figure 5* shows the stress-strain curves at 243 K which is below T_gs for all the samples. All the samples display brittle behaviour with stress-whitening.

The temperature dependence of tensile behaviour was summarized in *Table 2*. In this table, open circles represent ductile behaviour without stress-whitening, open triangles ductile behaviour with stress-whitening, and closed circles brittle behaviour with stress-whitening. Bold lines in the table denoted T_g region. The tensile behaviour of incompatible blends was independent of temperature. It is suggested that the fracture will be associated with the segregation occurred at the interface between PP and EBR domains. The blending of EBR56 and EBR62 was found to play a role of a plasticizer for i-PP. This will be because of the incorporation of the EBR molecules into the amorphous region of i-PP.

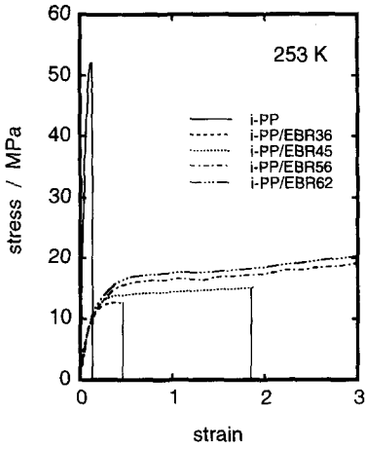

Figure 4 Stress-strain curves at 253 K for i-PP and i-PP/EBR blends

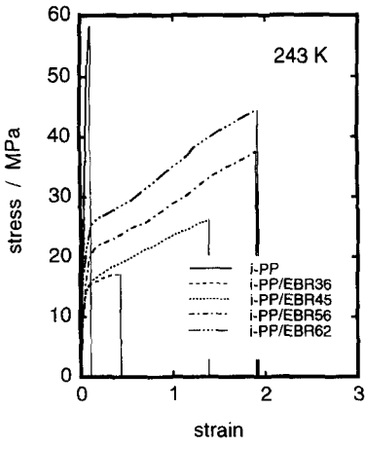

Figure 5 Stress-strain curves at 243 K for i-PP and i-PP/EBR blends

The strain rate dependence of stress-strain curves was examined in the range from 0.11 to 5.56% s^{-1}. The i-PP showed ductile behaviour with stress-whitening over the entire range of strain rate, suggesting that the plastic deformation occurs over the entire range of strain rate for i-PP. The compatible blends were ductile materials but showed a slight stress-whitening above strain rate of 0.56% s^{-1}. The incompatible blends showed brittle behaviour with stress-whitening irrespective of strain rate, suggesting that the segregation at interface between i-PP phase and EBR domains occurs in the entire range of the strain rate.

Rheo-optics

The orientation functions of chain axis as well as stress are plotted against the strain in *Figures 6–8*. *Figure 9* shows the strain dependence of the peak shifts $\Delta\nu$ of the 1168 cm^{-1} band. In these figures, the yielding point on the stress-strain curves is shown as point A. The point B in the stress-strain curves indicates a point at which the neck travels along the whole film specimen.

As seen in *Figure 6*, the orientation function of i-PP slightly decreases with increasing strain below the yielding (point A). The point A was almost equal to the strain at the stress-whitening. The orientation functions for both the 998 and 973 cm^{-1} bands monotonously increase beyond point A and level off in the vicinity of point B. It was found that the large difference in the orientation function between the 998 cm^{-1} crystal band and the 973 cm^{-1} amorphous band is seen in the region between A and B points. The 1168 cm^{-1} band of i-PP shifts to lower frequencies up to point A with increasing strain and approaches an equilibrium value as shown in *Figure 9*.

Table 2 Temperature dependence of tensile behaviour

Temp. (K)	i-PP	i-PP/ EBR36	i-PP/ EBR45	i-PP/ EBR56	i-PP/ EBR62
243	●	●	●	●	●
253	●	●	●	△	△
273	△	●	●	△	△
296	△	●	●	○	○
323	△	●	●	○	○

●: brittle with stress-whitening; △: ductile with stress-whitening; ○: ductile without stress-whitening

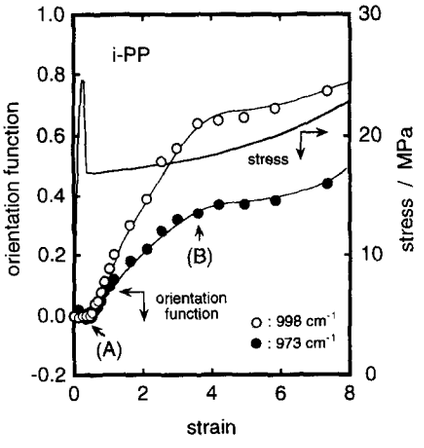

Figure 6 Strain dependence of orientation functions for 998 cm^{-1} and 973 cm^{-1} bands of i-PP, including the stress-strain curves

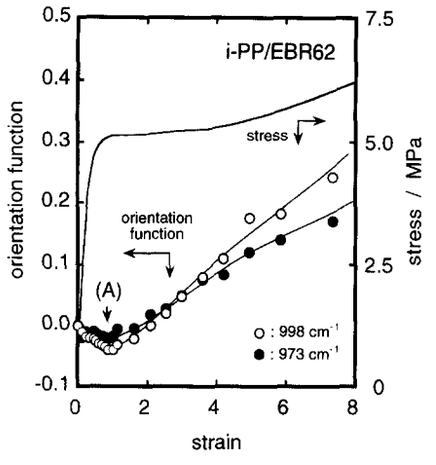

Figure 7 Strain dependence of orientation functions for 998 cm^{-1} and 973 cm^{-1} bands of compatible i-PP/EBR62 blends, including the stress-strain curves

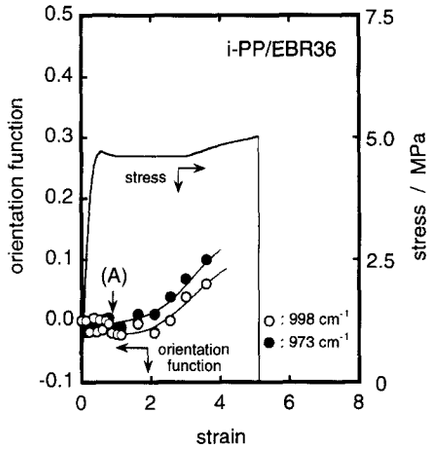

Figure 8 Strain dependence of orientation functions for 998 cm^{-1} and 973 cm^{-1} bands of incompatible i-PP/EBR36 blends, including the stress-strain curves

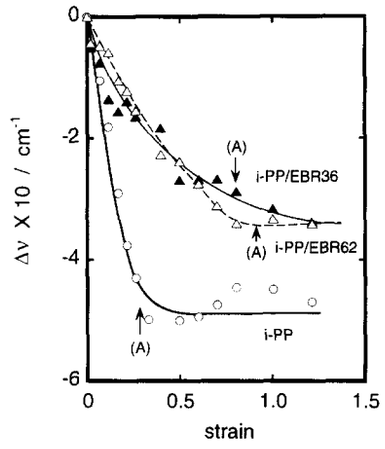

Figure 9 Frequency shift versus strain for 1168 cm^{-1} band of i-PP (open circles and a bold solid line), i-PP/EBR36 (closed triangles and a thin solid line), and i-PP/EBR62 (open triangles and a thin dashed line)

According to Onogi *et al.*[24–26] the deformation mechanism in crystalline polymers with well-developed spherulites was considered to be the following five processes as important factors: (1) the orientation of lamellae or the *b*-axis forced by the affine or pseudo affine deformation of spherulite; (2) the rearrangement and orientation of crystallites and fragmented lamellae caused by the twisting and/or slippage in lamellae, in which the chain axis (*c*-axis) orients parallel to the stretching direction; (3) the orientation of amorphous chain in the stretching direction; (4) the unfolding of folded chains and pulled-out chains from lamellae; (5) the microscopic disruption or plastic deformation such as dislocation, microvoids formation, craze, and crack.

In the initial strain region (below A point), the negative orientation can be explained by the mechanism (1), in which the lamellar orientation or the *b*-axis orientation caused the *c*-axis to orient perpendicular to the stretching direction. Therefore, the force required to produce the lamellar orientation exerts directly on the crystal of i-PP, resulting in the peak shift below point A. In the higher strain region above point A, the increase in orientation and the steady $\Delta\nu$ indicates that the mechanisms (3) and (4) occur beyond yielding process[27]. The deviation of the orientation of amorphous chains from that of crystal i-PP chains appeared at higher strains suggest that the mechanism (5) overcomes other mechanisms, leading the amorphous part to segregate from the crystal parts, and the effects of the mechanism (5) become progressively greater with increasing strain.

As seen in *Figure 7*, the orientation function of the 998 cm^{-1} band for compatible blend (i-PP/EBR62) shows a great decrease and then increases after passing a minimum around 1.0 (point A). The depth and location of i-PP/EBR62 are much larger than those of i-PP. Moreover, the orientation function of 998 cm^{-1}, together with the 973 cm^{-1} bands, increases with increasing strain. As seen in *Figure 9*, similarly with i-PP, $\Delta\nu$ of i-PP/EBR62 blend decreases and reaches an equilibrium after point A. The equilibrium values of $\Delta\nu$ are lower than that of i-PP, indicating that the force exerting on i-PP crystal, which will be responsible for the segregation between crystal and amorphous regions, is lowered by blending EBR56. These results on the orientation function and peak shifting for i-PP/EBR62 were almost the same with those for i-PP/EBR56.

These results suggest that the affine or pseudo affine deformation of spherulite dominantly occurs without any plastic deformation such as microvoids and craze for compatible i-PP/EBR blends. This is plausible because the rubbery EBR56 chains are incorporated into the amorphous region of i-PP, leading to decrease in T_g of amorphous i-PP chains. In contrast, in the case of i-PP homopolymer, the formation of microvoids and crazes in the initial strain region leads to the segregation between crystalline and amorphous phases in the higher strain region, resulting in the stress-whitening in the yielding region as well as the deviation of orientation of the crystal *c*-axis from that of amorphous chains in the post-yielding strain region.

The i-PP/EBR36 film was broken without orientation of both crystal and amorphous chains and the $\Delta\nu$ of the 1168 cm^{-1} band monotonously decreases with increasing strain beyond point A (see *Figures 8 and 9*). Similar results were also obtained for i-PP/EBR45. These results suggest that a macroscopic segregation occurs at interface between i-PP and EBR phases in the initial strain region, leading to a brittle fracture. In the case of such incompatible blends with phase separated domains, both the i-PP and EBR phases will deform simultaneously. Then the difference in Poisson ratio between i-PP and EBR36 probably leads to the phase segregation.

As is described in the experimental section, the initial slope in the $\Delta\nu$ versus strain curve can be related with

Table 3 Anharmonic Parameter for the 1168 cm^{-1} band

Sample	$\delta_G \times 10^2$
i-PP	14.7
i-PP/EBR36	9.3
i-PP/EBR45	12.0
i-PP/EBR56	6.0
i-PP/EBR62	4.3

Grüneisen constant γ_G. When $\Delta\sigma/b$ is assumed to be proportional to bulk (nominal) strain γ, anharmonic parameter δ_G, which is proportional to γ_G, can be estimated by equation (3);

$$\delta_G = -\left(\frac{dlnv_{1168}}{d\gamma}\right)_{\gamma=0} \quad (3)$$

The parameter δ_G can be a measure of anharmonicity or nonlinearity in molecular interaction concerning with stretching of i-PP backbone chains in crystalline region. Therefore, δ_G can be directly related to the mechanical nonlinearity and thermal expansion coefficient[28–31]. *Table 3* summarized the values of δ_G for i-PP and i-PP/EBR blends. It was found that the magnitude of δ_G is in the order of i-PP, i-PP/EBR36, and i-PP/EBR62. This is likely because the higher δ_G will be caused by the higher mechanical nonlinearity caused by the better formation of microvoids and craze during deformation of i-PP lamellae.

CONCLUSIONS

The tensile properties of i-PP and i-PP/EBR blends were investigated using a rheo-optical technique, in which the infrared absorbance and the stress were simultaneously measured during a constant rate of elongation. In the present study, we employed two kinds of the binary blends; i-PP with the 'ethylene rich' EBR and i-PP with the 'l-butene rich' EBR. The former is an incompatible blend showing a phase separation, and the latter is a compatible blend where EBR chains are incorporated into the amorphous region of i-PP.

In the case of compatible blends, spherulites are affinely deformed and plastic deformation hardly occurs during elongation. The incompatible blends show a brittle behaviour accompanied by segregation between i-PP and EBR phases. For i-PP homopolymer, microscopic disruption such as microvoids and crazes occurs in the initial strain region and the i-PP chains in lamellae and crystallites are much stressed.

ACKNOWLEDGEMENTS

The authors wish to express their gratitude to Profs M. Takayanagi and A. Tanaka for helpful suggestions.

REFERENCES

1. Polypropylene: Structure, Blends and Composites, ed. KargenKocsis J., Chapman & Hall, London, 1995.
2. Utracki, L. A., *Polymer Alloy and Blends*, Carl Hanser, Munich/FRG, 1989.
3. Gulli, P., Daresi, S. and Simouzzi, T., *Polym. Eng. Sci.*, 1984, **24**, 544.
4. Greco, R., Mancarella, C., Martuscelli, E., Ragosta, G. and Jinghua, Y., *Polymer*, 1929, **1987**, 28.
5. Martuscelli, E., *Polym. Eng. Sci.*, 1984, **24**, 563.
6. Rlaris, V. and Stachurski, Z. H. J., *Appl. Polym. Sci.*, 1992, **45**, 1789.
7. Yamaguchi, M., Miyata, H. and Nitta, K., *J. Appl. Polym. Sci.*, 1996, **62**, 87.
8. Stein, R. S., *New Methods of Polymer Characterization*, ed. Ke, Wiley, New York, 1968, p. 255.
9. Onogi, S., Asada, T. and Sakai, K., *Proc. 5th Int. Congr. Rheol*, Vol. 4, ed. Onogi, S., Univ. Tokyo and Univ. Park Press, Tokyo, 1970.
10. Wilkes, G. L., *Adv. Polym. Sci.*, 1971, **8**, 91.
11. Onogi, S., *Rheo-optical Studies of High Polymers*, Collection of Papers by S. Onogi, Kyoto Univ., Kyoto, 1971.
12. Siesler, H. W. and Hokkard-Moritz, K., *Infrared and Raman Spectroscopy of Polymers*, Marcel Dekker, New York, 1980.
13. Samuels, R. J., *The Science and Technology of Polymer Films*, ed. O. J. Sweeting, Wiley, New York, 1968, p. 255.
14. Fraser, R. D. D., *J. Chem. Phys.*, 1953, **21**, 1511.
15. Zbindem, R., *Infrared Spectroscopy of High Polymers*, Acad., New York, 1964, Chap. 5.
16. Onogi, S., Asada, T. and Tanaka, A., *J. Polym. Sci. A2*, 1969, 7, 171.
17. Miyazawa, T., *J. Polym. Sci. C*, 1964, **7**, 59.
18. Tadokoro, H., Kobayashi, M., Ukita, M., Yasufuku, K., Murahashi, S. and Torii, T., *J. Chem. Phys.*, 1965, **42**, 1432.
19. Lee, Y. L., Bretzlaff, R. S. and Wool, R. P., *J. Polym. Sci. Polym. Phys. Ed.*, 1984, **22**, 681.
20. Wool, R. P. and Boyd, R. H., *J. Appl. Phys.*, 1980, **51**, 5116.
21. Bretzlaff, R. S. and Wool, R. P., *J. Appl. Phys.*, 1980, **52**, 5964.
22. Kittel, C., *Introduction to Solid State Physics*, Wiley, New York, 1966.
23. Wool, R. P., Bretzlaff, R. S. and Boyd, R. H., *J. Polym. Sci. Polym. Phys. Ed.*, 1984, **24**, 1039.
24. Onogi, S., Fukui, Y. and Asada, T., *Proc. 5th Int. Congr. Rheol*, Vol. 4 (ed. S. Onogi), Univ. Tokyo and Univ. Park Press, Tokyo, 1970, p. 87.
25. Tanaka, A. and Onogi, S., *Polym. Eng. Rev.*, 1983, **3**, 235.
26. Tanaka, A., Fukuda, M., Nagai, H. and Onogi, S., *J. Polym. Sci. Polym. Phys. Ed.*, 1989, **27**, 2283.
27. Takayanagi, M. and Nitta, K., *Macromol. Theory Simul.*, 1997, **6**, 181.
28. Yamamoto, O., *Polym. J.*, 1971, **2**, 509.
29. Kijima, T., Koga, K., Imada, K. and Takayanagi, M., *Polym. J.*, 1975, **7**, 14.
30. Barron, R. M., Barron, T. H. K., Mummery, P. M. and Sharkey, M., *Can. J. Chem.*, 1988, **66**, 718.
31. Nitta, K., Uchida, Y. and Tanaka, A., *Polym. J.*, 1991, **23**, 895.